Hindawi
Geofluids
Volume 2022, Article ID 3021326, 7 pages
https://doi.org/10.1155/2022/3021326

WILEY | Hindawi

Research Article

NMR Analysis Method of Gas Flow Pattern in the Process of Shale Gas Depletion Development

Rui Shen, Zhiming Hu, Xianggang Duan, Wei Sun, Wei Xiong, and Hekun Guo

Research Institute of Petroleum Exploration & Development, PetroChina Company Limited, 20 Xueyuan Road, Haidian District, Beijing 100083, China

Correspondence should be addressed to Rui Shen; shenrui523@126.com

Received 6 July 2021; Accepted 16 December 2021; Published 10 January 2022

Academic Editor: Chenhao Sun

Shale gas reservoirs have pores of various sizes, in which gas flows in different patterns. The coexistence of multiple gas flow patterns is common. In order to quantitatively characterize the flow pattern in the process of shale gas depletion development, a physical simulation experiment of shale gas depletion development was designed, and a high-pressure on-line NMR analysis method of gas flow pattern in this process was proposed. The signal amplitudes of methane in pores of various sizes at different pressure levels were calculated according to the conversion relationship between the NMR T_2 relaxation time and pore radius, and then, the flow patterns of methane in pores of various sizes under different pore pressure conditions were analyzed as per the flow pattern determination criteria. It is found that there are three flow patterns in the process of shale gas depletion development, i.e., continuous medium flow, slip flow, and transitional flow, which account for 73.5%, 25.8%, and 0.7% of total gas flow, respectively. When the pore pressure is high, the continuous medium flow is dominant. With the gas production in shale reservoir, the pore pressure decreases, the Knudsen number increases, and the pore size range of slip flow zone and transitional flow zone expands. When the reservoir pressure is higher than the critical desorption pressure, the adsorbed gas is not desorbed intensively, and the produced gas is mainly free gas. When the reservoir pressure is lower than the critical desorption pressure, the adsorbed gas is gradually desorbed, and the proportion of desorbed gas in the produced gas gradually increases.

1. Introduction

Deep shale gas in China is abundant and owning an immense potential for exploitation, which is becoming a key area for shale gas production in future [1, 2]. The shale gas reservoir is a kind of unconventional gas reservoir, with ultralow porosity and ultralow permeability, being complex in pore structure [3]. A large number of pores with diameter smaller than 50 nanometers are well developed in shale gas reservoir [4–6]. In addition, microfractures and micron-sized pores also exist, with a storage space system of multi-scale. The gas in shale reservoirs is in a free or adsorbed state, with a complicated shale gas flow mechanism. According to the concentration of the gas, with Knudsen number (K_n), the gas flow can be divided into four types, including continuous flow, slip flow, transitional flow, and free molecular flow [7, 8]. The K_n is the ratio of the average molecular free path to the characteristic scale. The scale of pores in shale gas reservoirs varies significantly, resulting in different gas flowing patterns in different scale pores. However, there is a lack of the experimental method for quantitatively characterizing the pattern of shale gas flow in shale reservoirs.

NMR core analyzing method has been widely used in the field of oil and gas seepage mechanics, including the NMR porosity testing [9, 10], movable fluid saturation testing [11], water-driving-oil NMR analysis [12–17], gas-driving-oil NMR analysis [18], and NMR pore structure characterization [19–22]. When the study objects change from conventional reservoirs to unconventional reservoirs such as tight oil and shale oil reservoirs, the pore sizes are getting smaller and smaller, and the pore structures are becoming more and more complex. Particularly, large errors might occur when conducting the water-driving-oil and gas-driving-oil experiments on tight oil or shale oil cores with

conventional sampling method due to the very small flow rate. In contrast, with the online NMR method under high-temperature and high-pressure, the variation of fluid relaxation in the core can be monitored in real-time, allowing a more accurate measurement of the variation of oil and water in the core. Therefore, the application of NMR core analysis technology will be further expanded when studying the seepage mechanics for unconventional oil and gas reservoirs [23].

During shale gas depletion development experiment, combined with high-temperature and high-pressure online NMR analysis technology, the occurrence and recovering regulation of adsorbed and free gas can be analyzed. Some key parameters can be calculated from the experiment, such as the critical desorption pressure and the recovering proportion of adsorbed gas [24]. The above experiments have all suggested that the gas production from shale gas reservoirs decreased rapidly at the initial stage and became slow at the middle and late stages, which is consistent with the gas production in the actual production process of shale gas wells [25]. The critical desorption pressure of the shale gas from the Longmaxi Formation in the Sichuan Basin is 12-15 MPa. When the reservoir pressure is lower than this critical desorption pressure, the recoverable degree of adsorbed gas increases significantly. When the produced shale gas is mainly free gas, the recoverable degree of adsorbed gas is low.

The low magnetic field NMR T_2 spectrum distribution is directly related to the pore structure and can reflect the pore distribution of the sample to a certain extent [26, 27]. The key to study the pore size distribution with NMR test is to determine the surface relaxation rate and the shape of the pores. Generally, the surface relaxation rate is calculated by comparison with the capillary force curve obtained from the mercury intrusion capillary pressure experiment. By selecting an appropriate conversion coefficient (C), the capillary pressure curve can be coincided with the pseudo capillary pressure curve. The derivation process of an equation for the conversion of the NMR transverse relaxation time T_2 value to the throat radius was proposed. On an assumption that a linear relationship exists between $T_2$and the pore size distribution, the conversion coefficients of the NMR pore size distribution T_2 spectrum and the pore radius were calculated. Then, the NMR T_2 distribution was converted to the NMR capillary force curve, during which the value of the conversion coefficient (C_0) ranges from 33.3 to 250 [28–30]. As for the double-peak T_2 spectrum, two capillary pressure curves were separately constructed on both micropore and macropore segments by using two different power functions, and the linear method and power function method were used to construct the capillary pressure curve separately [31]. Li et al. proposed that under the condition of pore diameters less than 5 μm, the T_2-pore diameter relationship curves of the brine saturated sample and the oil-saturated sample are almost overlapped, indicating that the T_2 distribution is irrelevant with the fluid volume, but only associated with the pore size. In this case, no matter what fluid is saturated in the pores, the T_2 distribution is linearly related to the pore size distribution [32]. Hürlimann et al. determined the surface relaxation rate of sandstone and S/V value through diffusion experiment [33].

This paper presents an on-line NMR analysis method of flow pattern in the experimental process of shale gas depletion development. Specifically, the relative amplitude of methane in pores of various sizes under different pressure conditions is calculated according to the conversion relationship between T_2 spectrum and pore radius, and then, the flow patterns of methane in pores of various sizes under different pore pressure conditions are analyzed as per the flow pattern determination criteria. Application of this method is exemplified in the first submember of the first member of the Silurian Longmaxi Formation (L11) in Well Ning 203.

2. Materials and Methods

2.1. Experimental Methods. The shale core sample was collected from the Long11 submember of the Silurian Longmaxi Formation in Well Ning 203 in the Changning area of the Sichuan Basin. The core sample, with a length of 73.62 millimeters and a diameter of 25.72 millimeters, was taken from depth interval ranging from 2384.69 m to 2384.86 m. The porosity of the core sample is 6.07%, and the Klinkenberg permeability is 1.02 mD. To truly reveal the seepage characteristics of natural gas in the reservoir, methane gas with a purity of 99.99% was used during the experimental process. A high-temperature and high-pressure online NMR core analyzer (ReCore-2515), which is independently developed by the Seepage Fluid Mechanics research laboratory of Research Institute of Petroleum Exploration and Development, PetroChina, was used in this experiment. The experimental setup is shown in Figure 1.

The experiment includes four main steps. Firstly, dry the core sample at 105°C for 48 hours, cool it to room temperature in a drying dish, and put it into the holder. Secondly, test the air tightness of the system, open the inlet valve of the holder and close the outlet valve, evacuate the core until it reaches the vacuum requirements, and then close the vacuum pump valve. Thirdly, the methane gas is injected into the core, pressurized to 20 MPa, and fully saturated for 24 days to simulate the original occurrence state of adsorbed methane gas. The change of methane gas signal in the rock core is detected in real time during the saturation process. And the final equilibrium pressure is set at 18.26 MPa. When the inlet and outlet pressures no longer change after 96 hours, the core is considered to return to its original state. Due to the tightness and adsorption characteristics of the shale reservoir, this process might last up to tens of days. Finally, open the outlet, start the depletion development experiment, and record the NMR T_2 spectrum, the pressure at each measuring point, and gas production data at the outlet valve in real-time.

The experiment includes four main steps. (1) The core was dried at 105°C for 48 h and then cooled to 25°C in a drying dish before being put into a holder. (2) Check the tightness of the system. Open the inlet valve of the holder and close the outlet valve to vacuum the core. Close the inlet valve after reaching the vacuum requirement. (3) Methane gas is injected into the core in a constant pressure mode to

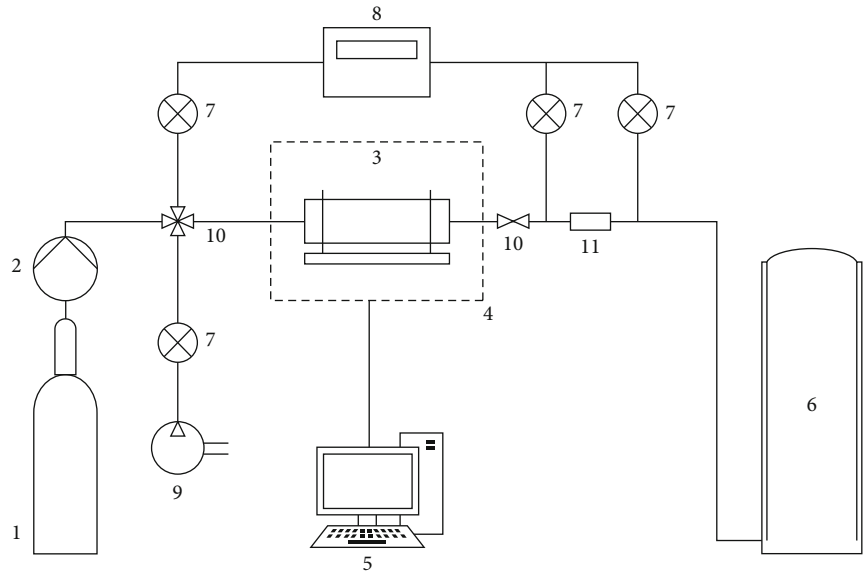

Figure 1: Flow diagram of the NMR experiment for analyzing shale gas depletion development.

restore the original reservoir occurrence. Record the pressure at both ends of the core and close the gas source after saturation to 18.26 MPa at the inlet and outlet of the core. When the inlet and outlet pressures do not change during 96 h, the core is restored to the original occurrence state. Due to the density and adsorption properties of shale reservoirs, this process can last for tens of days. (4) Open the outlet value, start the depletion development experiment. The data of T_2 spectrum, pressure at each measuring point, and gas production at outlet were recorded during the experiment.

2.2. NMR Pore Size Distribution. Low-magnetic-field NMR test results can provide abundant information on the fluid in porous media. In general, the relaxation time of fluid in porous media includes bulk relaxation, surface relaxation, and diffusion relaxation. In this study, the Carr-Purcell-Meiboom-Gill test sequence has been used, and only the surface relaxation needs to be considered [34, 35]. The relationship between the information of fluid in pores and relaxation time of the NMR test is shown in Equation (1):

$$\frac{1}{T_2} = \frac{1}{\rho_2}\frac{S}{V}, \tag{1}$$

where T_2 is the relaxation time, ms; ρ_2 is the surface relaxation rate, μm·ms^{-1}; and S/V is the ratio of specific surface area to pore volume, μm^{-1}.

According to Equation (1), small pores have larger S/V values. Therefore, small pores have shorter relaxation times than large pores. The relationship between the T_2 spectrum and the pore radius can be expressed by:

$$\frac{S}{V} = \frac{F_s}{d/2}, \tag{2}$$

where F_s is the shape factor of pores (3 for spherical pores and 2 for columnar pores), dimensionless, and d is the pore diameter, μm.According to Equation (1) and Equation (2), the relationship between the pre diameter (d) and the relaxation time (T_2) can be obtained:

$$d = CT_2, \tag{3}$$

where C is conversion coefficient set as 33 μm·ms^{-1} according to data range proposed in the literature [16].

2.3. Determination of the Flowing Pattern. Gas molecules frequently collide with each other during the movement process. The gas transportation process comes from the thermal motion of molecules. The collision causes the molecules to change continuously the direction and rate of movement, making the molecular movement path very tortuous. The collision also allows molecules to exchange continuously the energy and momentum, being the necessary prerequisites for the balance of the system. The path that the actual gas molecules travel between two collisions is called the free path. For gas molecules, the average distance between two

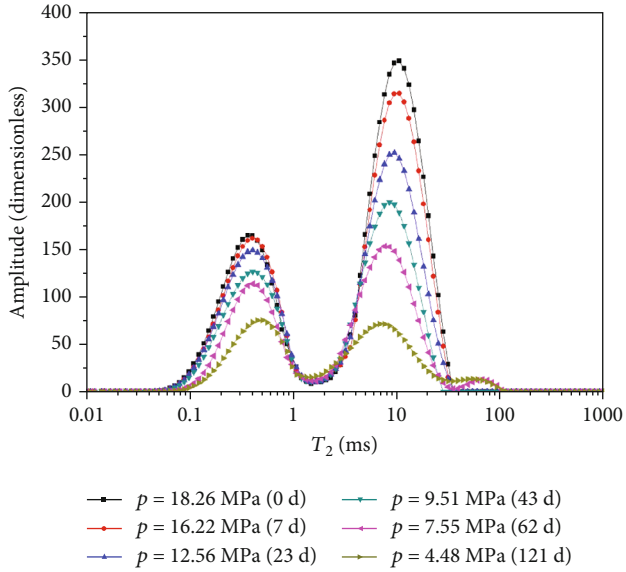

Figure 2: The T_2 spectrum distribution at different stages.

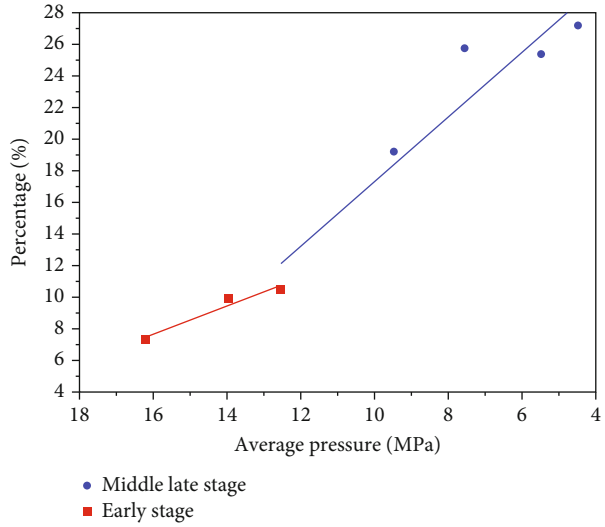

Figure 3: The proportion of adsorbed gas in the total produced gas at different average pore pressures.

adjacent collisions, known as the average free path of the molecule, is a physical quantity of only statistical significance, as shown in Equation (4) [36, 37]:

$$\lambda = \frac{k_B T}{\sqrt{2}\pi d_g^2 p}, \tag{4}$$

where d_g is the effective diameter of the molecule, μm; p is the gas pressure, MPa; k_B is the Boltzmann's constant, J/K; and T is the temperature, K.

Knudsen number (K_n) represents the ratio of the average free path of molecules (λ) to the characteristic length (L) of the object in the flow field.

3. Results and Discussion

3.1. Experimental Results. Figure 2 illustrates the T_2 spectrum distribution at six stages during the experiment, including at the beginning and when the experiment was carried out for 7, 23, 43, 62, and 121 days, respectively. At the beginning of the experiment, there are two peaks in the T_2 spectrum, and the signal amplitude of the right peak is about 1 times higher than that of the left peak, indicating that there are relatively many macropores in the shale core sample. The first 23 days of the experiment is equivalent to the initial stage of the experiment. As the average pore pressure of the core decreased, the signal amplitude corresponding to the right peak also decreased, but the signal amplitude corresponding to the left peak was almost unchanged, indicating that the gas recovered at the initial stage was mainly free gas in macropores, and the free gas and adsorbed gas in the mesopores and macropores were less recovered. This gas production law is in good accordance with the actual gas well production performance. When the experiment entered the middle and late stages, that is, 23 days after the experiment, the signal amplitude of the right peak and the left peak began to decrease simultaneously, indicating that the gas in the pores of all scales has been recovered. At present, it is generally believed that the adsorbed gas mainly exists in pores of nanoscale (i.e., pores with a pore size of smaller than 100 nanometers) [36]. According to Figure 2, the signal of the left peak varies slightly as the average pore pressure is higher than 12.6 MPa, indicating that the adsorbed gas has not been widely desorbed. When the average pore pressure is less than 12.6 MPa, the signal amplitude of the left peak begins to gradually decrease with the decrease of the average pore pressure, indicating that the critical desorption pressure is around 12.6 MPa, and the large-scale desorption of adsorbed gas only occurs when the pore pressure is lower than the critical desorption pressure. When the average pore pressure is greater than 12.6 MPa, the proportion of adsorbed gas in the total produced gas is less than 10%. With the production of methane from shale, the proportion of adsorbed gas in the total produced gas gradually increases, and it reaches 27.2% when the average pressure is 4.48 MPa, as shown in Figure 3.

3.2. Discussion of the Flowing Pattern of Shale Gas during the Depletion Development. According to Equation (3), the relaxation time at the horizontal axis in Figure 4 was converted into pore diameter. The average pressure of pores in the shale gas depletion development experiment dropped from 18.26 MPa to 4.48 MPa, and the NMR T_2 spectrum corresponding to the two pressure states is shown in the following figure. According to Equation (3), the molecular free paths were, respectively, calculated asp = 18.26 MPa and p = 4.48 MPa. The Knudsen number K_n is obtained by the ratio of molecular free path to characteristic scale. The flow state can be divided by the interval of K_n. That is, according to the degree of gas concentration, the flow can be divided into four regions based on K_n. This comprises continuous flow ($K_n < 0.01$), slip flow ($0.01 \le K_n < 0.1$), transitional flow ($0.1 \le K_n < 10$), and free molecular flow ($K_n \ge 10$) [8, 9].

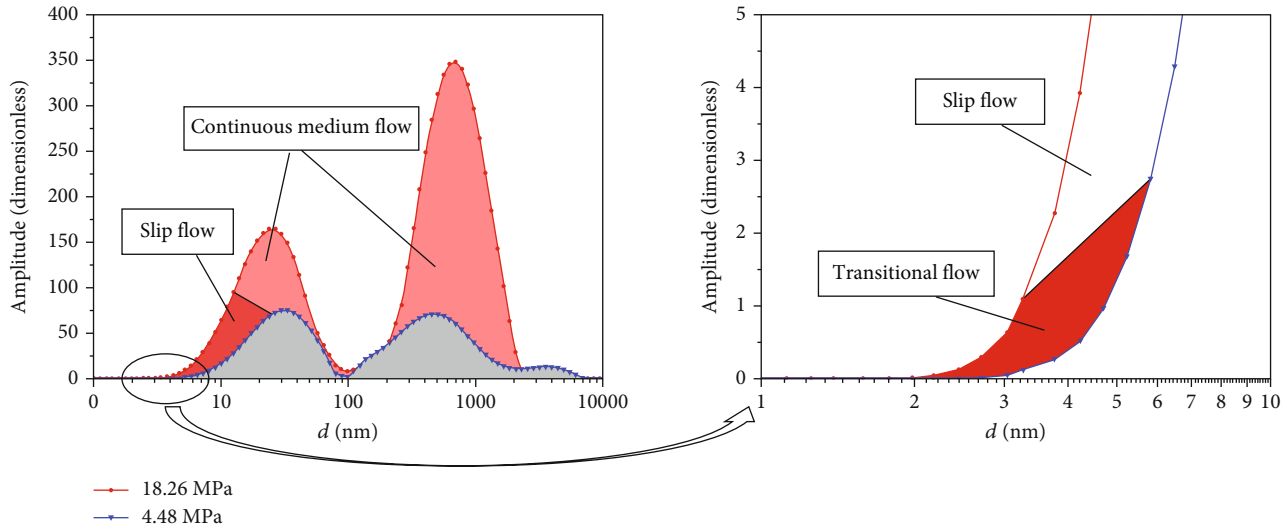

FIGURE 4: The amplitude distribution of the NMR signal corresponding to the pores of each scale under two pressure states at the beginning and end of the experiment (a) Full scale pore diameter distribution. (b) A magnified view of pore diameter 1-10 nm.

The nuclear magnetic resonance T_2 spectrum of methane saturated shale has obvious bimodal characteristics. Methane is mainly adsorbed on the surface of nanopores in shale. The adsorption is mainly controlled by surface relaxation. The relaxation time is short between 0.1 and 1.0 ms, and the main peak is 0.4 ms, corresponding to the left peak on the T_2 spectrum of NMR. Free methane exists in larger shale pores, which is not bound by pore wall, and has a long relaxation time which corresponds to the right peak on T_2 spectrum. The relaxation time is between 1 and 100 ms, and the main peak is 10 ms. Thus, the signal quantity of adsorbed/free state of methane gas in shale can be determined by T_2 spectrum. However, it is generally believed that the adsorbed gas mainly exists in pores of nanoscale (i.e., pores with a pore size less than 100 nanometers) [34]. Therefore, by calculating the ratio of the amplitude of the left peak to the total amplitude in the T_2 spectrum at the pressure of 18.26 MPa, the proportion of the adsorbed gas in the total gas in the initial state can be determined as 33.3%.

The free path of the gas molecule was calculated according to equation (3), and then, the K_n number was obtained by dividing it through the pore diameter. Figure 5 shows how the K_n number varies with the pore size at average pore pressure conditions of 18.26 MPa and 4.48 MPa, respectively. According to the criterion for determining flowing pattern, there are three flowing patterns, which include continuous flow, slip flow, and transitional flow during the shale gas depletion development experiment. When the average pore pressure of cores is 18.26 MPa, the pore size is less than 1.39 nm for transitional flow, 1.39–12.47 nm for slip flow, and more than 12.47 nm for continuous medium flow. When the average pore pressure is 4.48 MPa, the pore size is less than 5.81 nm for transitional flow, 5.81–57.1 nm for slip flow, and more than 57.1 nm for continuous medium flow. In Figure 4, the ratio of the area enveloped by the signal amplitude line for each flow pattern under each average pore pressure and the X-axis to the area enveloped by the whole signal amplitude line, and the X-axis is the proportion of the flow pattern under the average pore pressure.

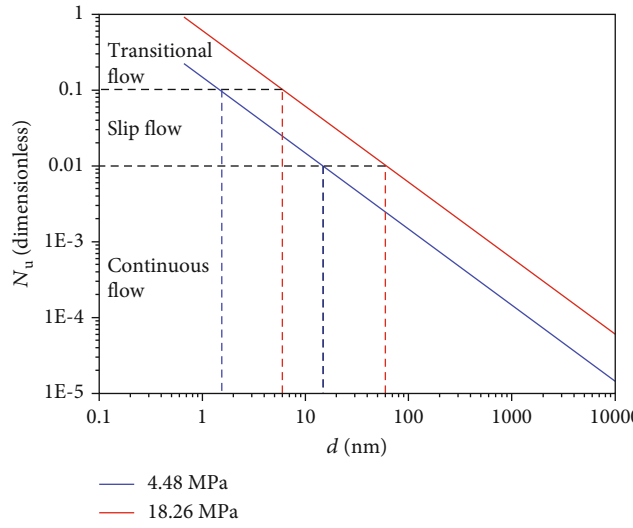

FIGURE 5: The distribution of K_n number under the pressure conditions at the beginning and end of the experiment.

Between Figures 4 and 5, it can be inferred that (1) when the pressure is 18.26 MPa, the flow pattern is mainly slip flow and continuous medium flow, with the former observed in pores with diameter of 1.39–12.47 nm, accounting for 6.1% of the total flow, and the latter in pores with diameter > 12.47 nm, that is, the Darcy flow, accounting for 93.9% of the total flow; and (2) when the pressure is 4.48 MPa, transitional flow occurs in the pores with diameter < 5.81 nm, accounting for 0.3% of the total flow; slip flow occurs in pores with diameter of 5.81–57.1 nm, accounting for 41.5% of the total flow; and continuous medium flow occurs in pores with diameter > 57.1 nm, accounting for 58.2% of the total flow.

Continuous medium flow is dominant at high pore pressure. However, it is important to note that continuous production in the shale reservoir results in a decrease in pore pressure, increase in Knudsen number, and an expansion of the pore size range of the slip flow zone and transitional zone, with both zones also being characterized by an increase in the proportion of diffusion flux to total flux. In the slip flow zone, there is a thin gas layer near the wall, that is, the Knudsen diffusion layer, and the flow in this zone needs to be simulated by the slip boundary conditions near the wall. In the transitional flow zone, the Knudsen diffusion layer is wider to trap most of the fluids, and the flow in this zone needs to be described by rarefied gas dynamics. The gas flow patterns obtained by NMR analysis are consistent with the findings in previous studies [36, 38], proving that the propose method is scientific and practical.

At present, there is little research on shale gas flow pattern analysis. For shale, a porous medium with large pore space scale span, usually only static flow pattern analysis under a certain pressure, is carried out. However, this is limited to flow pattern analysis under several characteristic scales. This study provides a dynamic analysis method of flow pattern in the process of depletion development. It is expected to be applied to the flow pattern analysis of depletion development of deep shale gas reservoirs under high reservoir pressure.

4. Conclusions

The on-line NMR analysis method of gas flow pattern can quantitatively analyze the gas flow patterns occurred under different pressure and pore size conditions in the process of shale gas depletion development and clarify the contribution of each flow pattern to the total flux in such process.

The shale gas depletion development experiment reveals three flow patterns: continuous medium flow, slip flow, and transitional flow. When the pore pressure is high, the continuous medium flow is dominant. With the decrease of pore pressure, the Knudsen number increases, and the pore size range of slip flow zone and transitional flow zone expands.

In the process of shale gas depletion development, there is a critical desorption pressure. When the reservoir pressure is higher than the critical desorption pressure, the adsorbed gas is not desorbed intensively, and the produced gas is mainly free gas. When the reservoir pressure is lower than the critical desorption pressure, the adsorbed gas is gradually desorbed, and the proportion of desorbed gas in the produced gas gradually increases.

Data Availability

Data available on request.

Conflicts of Interest

The authors declare no competing interests.

Acknowledgments

This paper is supported by the National Major Research Program for Science and Technology of China (2017ZX05037-001) and the Research Fund for Basic Research and Strategic Reserve Technology of Institutes Directly under CNPC (2018D-500806).

References

[1] W. Shen, X. Li, T. Ma, J. Cai, X. Lu, and S. Zhou, "High-pressure methane adsorption behavior on deep shales: experiments and modeling," *Physics of Fluids*, vol. 33, no. 6, article 063103, 2021.

[2] X. Guo, D. Hu, Y. Li et al., "Theoretical progress and key technologies of onshore ultra-deep oil/gas exploration," *Engineering*, vol. 5, no. 3, pp. 458–470, 2019.

[3] X. Ma, J. Xie, and R. Yong, "Geological characteristics and high production control factors of shale gas reservoirs in Silurian Longmaxi Formation, southern Sichuan Basin, SW China," *Petroleum Exploration and Development*, vol. 47, no. 5, pp. 901–915, 2020.

[4] Y. Wang, H. Wang, C. Zhang, X. Li, and D. Dong, "Fracture pore evaluation of the Upper Ordovician Wufeng to Lower Silurian Longmaxi Formations in southern Sichuan Basin, SW China," *Petroleum Exploration and Development*, vol. 44, no. 4, pp. 563–572, 2017.

[5] Y. Li, X. Liu, S. Gao et al., "A generalized model for gas flow prediction in shale matrix with deduced coupling coefficients and its macroscopic form based on real shale pore size distribution experiments," *Journal of Petroleum Science and Engineering*, vol. 187, article 106712, 2020.

[6] Y. Zhao, L. Peng, S. Liu, B. Cao, Y. Sun, and B. Hou, "Pore structure characterization of shales using synchrotron SAXS and NMR cryoporometry," *Marine and Petroleum Geology*, vol. 102, pp. 116–125, 2019.

[7] Y. Liu, Y. Yao, D. Liu, S. Zheng, G. Sun, and Y. Chang, "Shale pore size classification: an NMR fluid typing method," *Marine and Petroleum Geology*, vol. 96, pp. 591–601, 2018.

[8] M. Knudsen, "Die Gesetze der Molekularströmung und der inneren Reibungsströmung der Gase durch Röhren," *Annalen der Physik*, vol. 333, no. 1, pp. 75–130, 1909.

[9] Y. Wu, K. Pruess, and P. Persoff, "Gas flow in porous media with Klinkenberg effects," *Transport in Porous Media*, vol. 32, no. 1, pp. 117–137, 1998.

[10] X. Li, Y. Kang, and M. Haghighi, "Investigation of pore size distributions of coals with different structures by nuclear magnetic resonance (NMR) and mercury intrusion porosimetry (MIP)," *Measurement*, vol. 116, pp. 122–128, 2018.

[11] J. Li, S. Lu, G. Chen, M. Wang, S. Tian, and Z. Guo, "A new method for measuring shale porosity with low-field nuclear magnetic resonance considering non-fluid signals," *Marine and Petroleum Geology*, vol. 102, pp. 535–543, 2019.

[12] M. Appel, "Nuclear magnetic resonance and formation porosity," *Petrophysics*, vol. 45, no. 3, pp. 296–307, 2004.

[13] Y. Song and R. Kausik, "NMR application in unconventional shale reservoirs - a new porous media research frontier," *Progress in Nuclear Magnetic Resonance Spectroscopy*, vol. 112-113, pp. 17–33, 2019.

[14] Z. Liu, D. Liu, Y. Cai, Y. Yao, Z. Pan, and Y. Zhou, "Application of nuclear magnetic resonance (NMR) in coalbed methane and shale reservoirs: a review," *International Journal of Coal Geology*, vol. 218, article 103261, 2020.

[15] J. Liu and J. Sheng, "Experimental investigation of surfactant enhanced spontaneous imbibition in Chinese shale oil reservoirs using NMR tests," *Journal of Industrial and Engineering Chemistry*, vol. 72, pp. 414–422, 2019.

[16] C. Dai, R. Cheng, X. Sun et al., "Oil migration in nanometer to micrometer sized pores of tight oil sandstone during dynamic surfactant imbibition with online NMR," *Fuel*, vol. 245, pp. 544–553, 2019.

[17] P. Zhang, S. Lu, J. Li, C. Chen, H. Xue, and J. Zhang, "Petrophysical characterization of oil-bearing shales by low-field nuclear magnetic resonance (NMR)," *Marine and Petroleum Geology*, vol. 89, pp. 775–785, 2018.

[18] I. Gupta, C. Rai, and C. Sondergeld, "Study impact of sample treatment and insitu fluids on shale wettability measurement using NMR," *Journal of Petroleum Science and Engineering*, vol. 176, pp. 352–361, 2019.

[19] S. Su, Z. Jiang, X. Shan et al., "The wettability of shale by NMR measurements and its controlling factors," *Journal of Petroleum Science and Engineering*, vol. 169, pp. 309–316, 2018.

[20] Y. Yuan and R. Rezaee, "Fractal analysis of the pore structure for clay bound water and potential gas storage in shales based on NMR and N_2 gas adsorption," *Journal of Petroleum Science and Engineering*, vol. 177, pp. 756–765, 2019.

[21] Y. Volokitin, W. Looyestijn, W. Slijkerman, J. Hofman, X. Jing, and L. Riepe, "A practical approach to obtain primary drainage capillary pressure curves from NMR core and log data," *Petrophysics*, vol. 42, no. 4, pp. 334–343, 2001.

[22] W. Sun, Y. Zuo, Z. Wu et al., "Fractal analysis of pores and the pore structure of the lower Cambrian Niutitang shale in northern Guizhou province: investigations using NMR, SEM and image analyses," *Marine and Petroleum Geology*, vol. 99, pp. 416–428, 2019.

[23] E. Silletta, M. Franzoni, G. Monti, and R. Acosta, "Influence of exchange in NMR pore size/relaxation correlation experiments," *Microporous and Mesoporous Materials*, vol. 269, pp. 17–20, 2018.

[24] S. Zhang, J. Yan, Q. Hu et al., "Integrated NMR and FE-SEM methods for pore structure characterization of Shahejie shale from the Dongying Depression, Bohai Bay Basin," *Marine and Petroleum Geology*, vol. 100, pp. 85–94, 2019.

[25] X. Ma, S. Guo, D. Shi, Z. Zhou, and G. Liu, "Investigation of pore structure and fractal characteristics of marine- continental transitional shales from Longtan Formation using MICP, gas adsorption, and NMR (Guizhou, China)," *Marine and Petroleum Geology*, vol. 107, pp. 555–571, 2019.

[26] Y. Yao, J. Liu, D. Liu, J. Chen, and Z. Pan, "A new application of NMR in characterization of multiphase methane and adsorption capacity of shale," *International Journal of Coal Geology*, vol. 201, pp. 76–85, 2019.

[27] M. Testamanti and R. Rezaee, "Considerations for the acquisition and inversion of NMR T_2 data in shales," *Journal of Petroleum Science and Engineering*, vol. 174, pp. 177–188, 2019.

[28] M. Tan, K. Mao, X. Song, X. Yang, and J. Xu, "NMR petrophysical interpretation method of gas shale based on core NMR experiment," *Journal of Petroleum Science and Engineering*, vol. 136, pp. 100–111, 2015.

[29] M. Fleury and M. Romero-Sarmiento, "Characterization of shales using T_1- T_2 NMR maps," *Journal of Petroleum Science and Engineering*, vol. 137, pp. 55–62, 2016.

[30] P. Zhao, L. Wang, C. Xu et al., "Nuclear magnetic resonance surface relaxivity and its advanced application in calculating pore size distributions," *Marine and Petroleum Geology*, vol. 111, pp. 66–74, 2020.

[31] S. Zheng, Y. Yao, D. Liu, Y. Cai, and Y. Liu, "Nuclear magnetic resonance surface relaxivity of coals," *International Journal of Coal Geology*, vol. 205, pp. 1–13, 2019.

[32] J. Li, W. Jin, L. Wang, Q. Wu, and J. Lu, "Quantitative relationship between NMR T_2 and pore size of shale gas reservoir from core experiment," *Well Logging Technology*, vol. 40, no. 4, pp. 460–464, 2016.

[33] M. Hürlimann, L. Latour, and C. Sotak, "Diffusion measurement in sandstone core: NMR determination of surface-to-volume ratio and surface relaxivity," *Magnetic Resonance Imaging*, vol. 12, no. 2, pp. 325–327, 1994.

[34] J. Lai, S. Wang, C. Zhang et al., "Spectrum of pore types and networks in the deep Cambrian to Lower Ordovician dolostones in Tarim Basin, China," *Marine and Petroleum Geology*, vol. 112, article 104081, 2020.

[35] J. Lai, G. Wang, Z. Wang et al., "A review on pore structure characterization in tight sandstones," *Earth-Science Reviews*, vol. 177, pp. 436–457, 2018.

[36] F. Javadpour, D. Fisher, and M. Unsworth, "Nanoscale gas flow in shale gas sediments," *Journal of Canada Petroleum Technology*, vol. 46, no. 10, pp. 55–61, 2007.

[37] W. Shen, F. Song, X. Hu, G. Zhu, and W. Zhu, "Experimental study on flow characteristics of gas transport in micro- and nanoscale pores," *Scientific Reports*, vol. 9, no. 1, p. 10196, 2019.

[38] S. Muncaci, I. Ardelean, and S. Boboia, "The effect of diffusion in internal gradients on nuclear magnetic resonance transverse relaxation measurements," *AIP Conference Proceedings*, vol. 1565, pp. 133–136, 2013.